ORGANOMETALLICS

pubs.acs.org/Organometallics Article

σ/π Plasticity of NHCs on the Ruthenium−Phosphine and Ruthenium═Ylidene Bonds in Olefin Metathesis Catalysts

Luis Miguel Azofra,* Sai V. C. Vummaleti, Ziyun Zhang, Albert Poater,* and Luigi Cavallo*

Cite This: *Organometallics* 2020, 39, 3972−3982 Read Online

ACCESS | Metrics & More | Article Recommendations | Supporting Information

ABSTRACT: The nature of the Ru bonding environment in a set of Grubbs catalysts has been studied by means of density functional theory (DFT). On the one hand, for a set of 20 $[Ru(=CH_2)(NHC)(PCy_3)][Cl]_2$ second-generation adducts, the results show that calculated ^{31}P NMR shieldings exhibit a good correlation with the calculated R(Ru−P) bond lengths, which are in turn strongly correlated with the calculated PCy_3 ligand dissociation energies. Bond energy decomposition analysis (EDA) also indicates that there is a strong correlation between the σ and π orbital interaction energies for the Ru−PCy_3 bond, while no correlation was found for the case of the bond between the Ru moiety and the N-heterocyclic carbene (NHC) ligands, Ru−NHC. Furthermore, π orbital interaction energies of the Ru−PCy_3 bond were found to be strongly correlated with the calculated PCy_3 ligand dissociation energies, as well as with the R(Ru−P) bond lengths, confirming the significance of the π back-donation component from Ru to PCy_3 in determining the lability of the PCy_3 ligand in the studied adducts. On the other, for a set of 17 $[Ru(=CHR)(NHC)_x(PCy_3)_{2-x}][Cl]_2$ first (x = 0)- and second-generation (x = 1) complexes, DFT results show that changes occurring in the ^{13}C NMR shielding of the Ru═ylidene bond are mainly due to σ(Ru═C) → π*(Ru═C) molecular orbital (MO) transitions. Good correlations are observed between σ(^{13}C) and the energy gaps of the MOs involved in such transitions, between the binding energies of the ylidene moiety and the rest of the Ru fragment, as well as with the R(Ru═C) bond lengths. Finally, our novel preliminary results suggest that, once the metallacycle intermediate is formed by reaction with ethylene, $^{13}C'(\beta)$ NMR shielding retains the NMR information from σ(^{13}C) in the 16e species, in contrast to what happens with the $^{13}C(\alpha)$ NMR shielding.

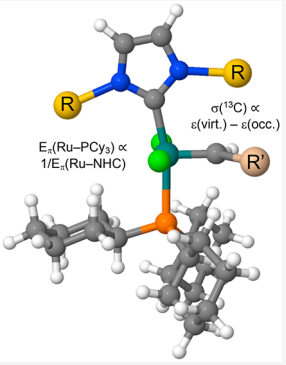

INTRODUCTION

In the less than three decades since Arduengo reported the synthesis of the first crystalline N-heterocyclic carbene (NHC),[1] the use of this organic species as a ligand in organometallic complexes has increased exponentially.[2] In a mimetic manner, NHCs have often been a perfect substitute for phosphines in organometallic catalysts, in which changes in the steric and/or electronic properties[3] have resulted in an improved catalytic activity.

Apart from the recent advances in organocatalysis,[4] the effect of the NHCs in catalysis has been basically circumscribed when they are linked to metals.[5] Particularly, as a ligand of organometallic complexes, the inclusion of an NHC ligand by Grubbs in exchange for a phosphine provoked the definitive impulse for the olefin metathesis to be recognized soon after, in 2005, with the Nobel Prize,[6] together with Chauvin[7] and Schrock.[8] Further, this represented the switch from first-[9] to second-generation Grubbs catalysts.[10]

Several methods have been developed for the characterization and rationalization of specific properties in NHC ligands, with special emphasis on the electronic and steric properties,[11] such as the Tolman electronic parameter (TEP)[12] and the percent buried volume (%V_{bur}).[13] In this context, the metal−ligand electronic parameter (MLEP) also includes the metal in the analysis,[14] apart from the extended view that steric maps also provide.[15]

With regard to the electronic part, NHCs have been assumed to be purely σ donors,[5g,16] although subsequent studies confirmed that the contributions of π bonding are not insignificant.[3a,17] In this context, while the σ donor effect in NHCs is prominent, an important dose of π back-donation is observed when NHCs are complexed, thus accepting electron density or even behaving as π donor agents.[18]

Scheme 1a exemplifies how the back-donation works with any metal (M),[19] involving a d orbital of M and the π* orbital from the NHC. Actually, it consists of the in-phase combination between a filled d orbital on the metal with an empty π* orbital of the NHC, whereas the interaction of the same orbitals also generates the corresponding antibonding orbital.[20]

Received: August 11, 2020
Published: November 12, 2020

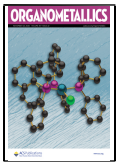

https://dx.doi.org/10.1021/acs.organomet.0c00536
Organometallics 2020, 39, 3972−3982

Scheme 1. (a) Simple Representation of the Frontier Molecular Orbitals involving the M(d) and NHC(π) Orbitals[a] and (b) Previously Studied Systems[20] and Overview of this Investigation

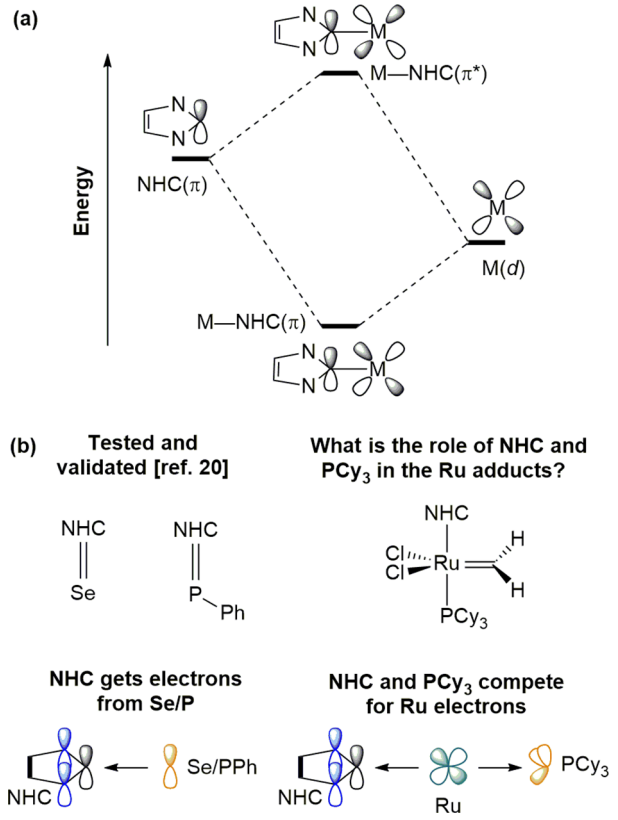

[a]Ru to NHC back-bonding gathers a filled d orbital on Ru with an empty π orbital of the NHC (M refers to metal).

With regard to the π bonding nature of NHCs, Nolan,[21] Bertrand,[22] and Ganter[23] overcame small inconsistencies of the TEP using NMR coupling constants on the Pt−C bond for $[PtCl_2(DMSO)(NHC)]$ complexes and the phosphorus and selenium signals of phosphinidene adducts[24] and selenourea compounds, respectively. In this context, Nolan and co-workers also probed the π back-bonding abilities to NHC of phosphinidene and selenium adducts and the capabilities of selenoureas to be deployed as ligands for Au(I).[25]

The theoretical interpretation derived from these compounds is insufficient, and therefore it is not fully valid for metallic complexes bearing NHC ligands,[3] only for NHC=PPh and NHC=Se.[20] In this sense, Belpassi and Zuccaccia examined the σ donation and the π back-donation in Au(NHC)-based complexes, taking into account the *trans* ligand to the NHC,[26] continuing the work of Ciancaleoni and Belpassi in the same sense, although the latter only considered the use of phosphine ligands.[27] More recently, the π back-donation has been analyzed to distinguish between cationic Au-NHC complexes and their isolobal NHC-proton compounds.[28] However, for the case of Grubbs olefin metathesis catalysts, in order to properly define the NHC ligand, its description should be in combination with, at least, the *trans* Ru−P bond.

Thus, in order to understand the nature of the Ru−P and Ru−NHC bonds, and also to shed light onto the mode of communication between the phosphine (PCy_3) and NHC ligands (Scheme 1b), a total of 20 $[Ru(=CH_2)(NHC)(PCy_3)][Cl]_2$ second-generation adducts (Figure 1), of which 14 contain standard NHCs covering derivatives of imidazol-2-ylidenes and 4,5-dihydroimidazol-2-ylidenes, 3 include triazol-2-ylidene carbenes, and 3 contain cyclic alkylaminocarbenes (CAAC), were investigated. In a second part, an analysis of the bonding and NMR properties for the Ru=ylidene bond has been performed for a set of 17 $[Ru(=CHR)(NHC)_x(PCy_3)_{2-x}][Cl]_2$ first (x = 0)- and second-generation

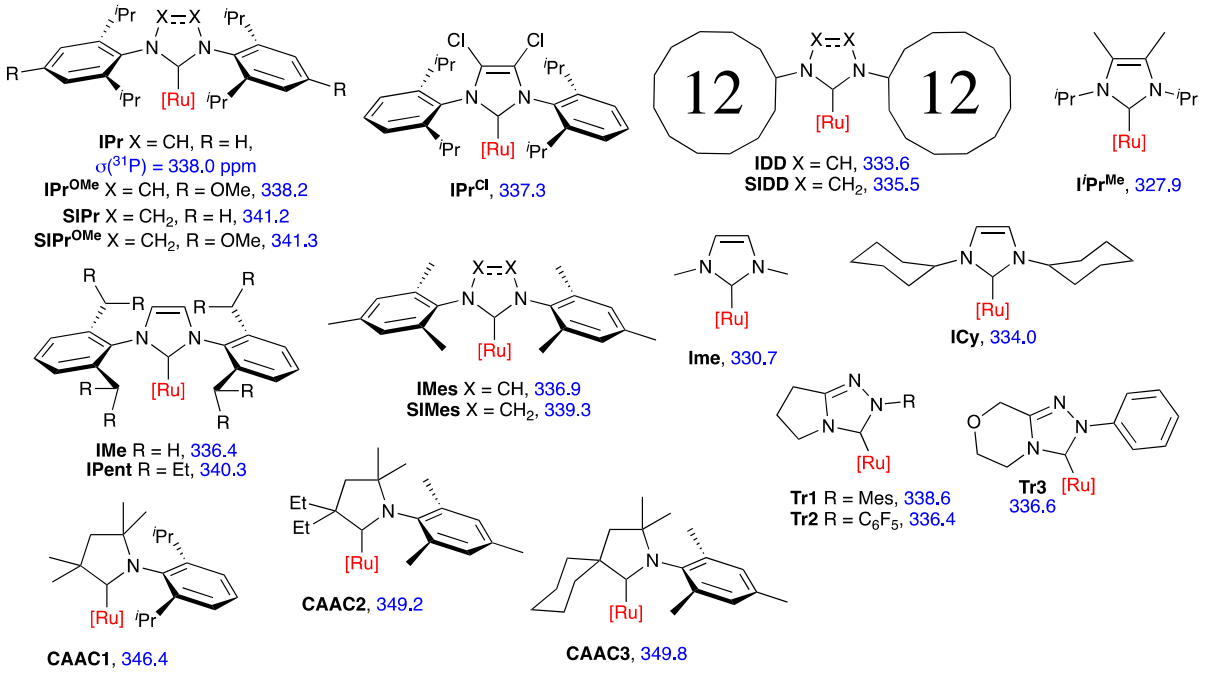

Figure 1. Set of 20 $[Ru(=CH_2)(NHC)(PCy_3)][Cl]_2$ second-generation adducts considered in the first part of this study, where [Ru] (red) = $[Ru(=CH_2)(PCy_3)][Cl_2]$ and ^{31}P magnetic shieldings, $\sigma(^{31}P)$, are shown in ppm (blue).

https://dx.doi.org/10.1021/acs.organomet.0c00536
Organometallics 2020, 39, 3972−3982

(x = 1) Grubbs catalysts, in which different ylidene moieties, =CHR, from previously synthesized complexes have been studied (*vide infra*, Figure 7). In this sense, our objective is to provide a comprehensive view of the connectivity between the most important functional groups linked to the central metal atom in ruthenium-based olefin metathesis catalysts: i.e., what is the communication mode in terms of energy, orbital, and NMR analysis?

COMPUTATIONAL DETAILS

The structures and energies for a set of second-generation [Ru(=CH_2)(NHC)(PCy_3)][Cl]$_2$ and first (x = 0)- and second-generation (x = 1) [Ru(=CHR)(NHC)$_x$(PCy_3)$_{2-x}$][Cl]$_2$ Grubbs catalysts have been studied through the use of density functional theory (DFT) *via* the spin-restricted Kohn–Sham (RKS) formalism. The generalized gradient approximation (GGA) has been used *via* the BP86 functional[29] together with the TZ2P Slater-type orbital (STO) basis set,[30] which is augmented by one polarization function for both light (hydrogen) and heavy atoms. The DIIS procedure was applied for the self-consistent field (SCF) convergence with the Becke fuzzy cell integration scheme (quality good).[31]

The zeroth order regular approximation (ZORA)[32] to the Dirac equation was applied during the optimization calculations in the gas phase in order to include relativistic effects (scalar) and freeze the inner-core orbitals. Nuclear magnetic resonance (NMR) chemical shifts were calculated using the gauge-including atomic orbitals (GIAO) method[33] through all-electron basis sets and inclusion of relativistic spin–orbit coupling.

Energy decomposition analysis (EDA)[34] has been performed over C_s-symmetrized complexes by rigid fragmentation into the two respective moieties. In the framework of EDA, the total binding energy (BE) is divided into deformation energy and interaction energy (BE = ΔE_{int} + ΔE_{def}). The interaction energy (ΔE_{int}) is the energy released when the two free deformed fragments are brought to the position that they have in the joint complex between both moieties, whereas the deformation energy (ΔE_{def}) is the energy needed to modify the geometry of the ground state free fragments to attain the geometry that they have together. Next, in a second decomposable level ΔE_{int} can be split into electrostatic, Pauli repulsion, and orbital interaction terms (ΔE_{int} = ΔE_{elstat} + ΔE_{Pauli} + ΔE_{oi}). The attractive term ΔE_{elstat} corresponds to the classical electrostatic interaction between the unperturbed charge distributions of the prepared fragments. The also attractive orbital interaction term, ΔE_{oi}, accounts for charge transfer and polarization, while the repulsive Pauli term, ΔE_{Pauli}, comprises the destabilizing interactions between occupied orbitals and is responsible for the steric repulsion. In the present study, we will focus on an analysis of values derived from ΔE_{oi}.

All calculations were carried out through the facilities provided by the Amsterdam Density Functional (ADF) modeling suite package (revision 2016.102).

RESULTS AND DISCUSSION

Ruthenium–Phosphine Bond. The calculated magnetic shielding of the P atom in the 20 complexes of Figure 1 spans a window of 21.9 ppm, with the complexes **CAAC3** and **I^{i}Pr^{Me}** presenting the highest and lowest calculated ^{31}P magnetic shielding (349.8 vs 327.9 ppm, respectively). This narrow range is somewhat surprising, despite the fact that the considered N-heterocyclic carbenes (NHC) are remarkably different in terms of both steric and electronic properties. In detail, unsaturated imidazol-2-ylidenes bearing secondary alkyl N substituents exhibit the lowest DFT calculated ^{31}P magnetic shielding (328–334 ppm), followed by unsaturated *N*,*N*′-diarylimidazol-2-ylidenes and one example of a saturated *N*,*N*′-dialkyl-4,5-dihydroimidazol-2-ylidene (335–338 ppm). Triazoles also appear in the same region. On the other hand, saturated *N*,*N*′-diaryl species exhibit higher σ(^{31}P) values (339–341 ppm). Interestingly, **CAAC** complexes exhibit the highest ^{31}P magnetic shielding (346–350 ppm).

Decomposition of the total isotropic magnetic shielding into paramagnetic and diamagnetic terms (plus spin–orbit),[35] σ = σ_p + σ_d (+σ_{SO}), indicates that the main variable is the paramagnetic shielding term, σ_p, which varies over a range of 22 ppm, while the diamagnetic shielding term σ_d covers a range of only 2 ppm (see Table S1 in the Supporting Information). This observation is consistent with our recent findings for selenoureas and phosphinidine adducts.[20]

We start the analysis by examining the correlation between the ^{31}P magnetic shielding and one of the most trivial geometrical parameters in these complexes, the Ru–PCy_3 distance. As shown in Figure 2, an excellent correlation (R^2 = 0.88) is obtained, with higher magnetic shielding corresponding to longer Ru–PCy_3 distances. A point worth mentioning here is that, similarly to the calculated magnetic shielding of the P atom, Ru–PCy_3 distances also span a rather small window of about 0.12 Å.[36] On the other hand, we did not find any reasonable correlation between the Ru–PCy_3 and the Ru–NHC distances and, consequently, between the Ru–NHC distance and the calculated ^{31}P shielding, with R^2 values of 0.59 and 0.53, respectively (see Figure S1 in the Supporting Information).

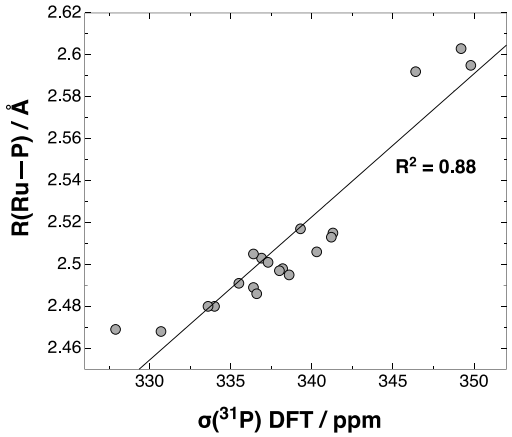

Figure 2. Calculated ^{31}P magnetic shielding, σ(^{31}P), vs the distance between the Ru and P atoms, R(Ru–P), in the ruthenium complexes shown in Figure 1.

The calculated R(Ru–P) and R(Ru–C) distances can be good indicators of the corresponding bond strengths. Therefore, we estimated the Ru–PCy_3 and Ru–NHC bond energies as the ligand dissociation energies (ΔE_L, where L = PCy_3, NHC), i.e., the difference in potential energies of the optimized geometries of products and reactants, as shown in eqs 1 and 2:

$$\Delta E_{PCy3} = (E_{[NHC-Ru(CH2)(Cl)2]} + E_{PCy3}) - (E_{[NHC-Ru(CH2)(Cl)2-PCy3]}) \quad (1)$$

$$\Delta E_{NHC} = (E_{[Ru(CH2)(Cl)2-PCy3]} + E_{NHC}) - (E_{[NHC-Ru(CH2)(Cl)2-PCy3]}) \quad (2)$$

For the 20 ruthenium adducts studied, in a plot of the calculated ΔE_{PCy3} vs R(Ru–P), a strong correlation (R^2 =

https://dx.doi.org/10.1021/acs.organomet.0c00536
Organometallics 2020, 39, 3972–3982

0.86) is gratifyingly achieved (Figure 3). In contrast, no correlation (R^2 = 0.09) was observed for the calculated ΔE_{NHC}

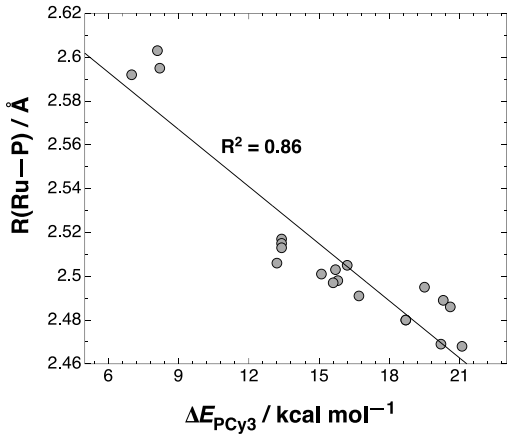

Figure 3. Interatomic distance between the Ru and P atoms, R(Ru−P), vs. calculated Ru−PCy_3 dissociation energies, ΔE_{PCy3}, in the ruthenium complexes shown in Figure 1.

vs R(Ru−C) (Figure S2 in the Supporting Information). This observation can be attributed to the fact that different NHCs presented in the considered ruthenium adducts possess different steric and electronic properties, which strongly influence the coordination of NHC to the Ru metal and thus the strength of the Ru−NHC bond.

At this point, a bond energy decomposition analysis (EDA) of the considered ruthenium adducts, rigidly fragmented into the $[Ru(=CH_2)(NHC)][Cl]_2$ and PCy_3 moieties and the $[Ru(=CH_2)(PCy_3)][Cl]_2$ and NHC moieties, was performed to unravel the nature of the Ru−PCy_3 and Ru−NHC bonds, with the main focus on the extent of π back-donation from a filled Ru d_z orbital to the empty PCy_3 or NHC π^* orbital. To this end, the geometries of all the complexes were reoptimized under the constraint of C_s symmetry, with the NHC ring lying in the σ_{xy} plane. This allows the orbital interaction energy contribution of the A' and A'' irreducible representations to be associated with the σ and π Ru−PCy_3 and Ru−NHC bonds (E_σ and E_π), respectively. Focusing on the nature of the Ru−PCy_3 bond in Figure 4a, we found an excellent correlation (R^2 = 0.93) between $E_\sigma(PCy_3 \rightarrow Ru)$ and E_π(Ru-PCy_3), indicating that a stronger Ru−PCy_3 σ bond means a stronger Ru−PCy_3 π bond. On the other hand, for the Ru−NHC bond, in Figure 4b correlating E_σ(NHC → Ru) vs E_π(Ru → NHC) there was a poor correlation (R^2 = 0.23), which is in line with our earlier findings for selenoureas and phosphinidine adducts.[20] Additionally, we observed an excellent correlation (R^2 = 0.94) between E_π(Ru → PCy_3) and the calculated ^{31}P magnetic shielding (see Figure S3 in the Supporting Information).

With these insights into the nature of the Ru−PCy_3 and the Ru−NHC bonds in hand, we then explored the mode of communication between PCy_3 and NHC ligands interconnected *via* the Ru metal. Figure 5 shows those orbitals of each moiety involved in the σ and π bonding of the Ru−PCy_3 and Ru−NHC bonds. Then, we searched for a correlation between the estimated E_σ and E_π of Ru−PCy_3 and Ru−NHC bonds (Figure 6); a strong correlation (R^2 = 0.91) was observed between E_π(Ru → NHC) and E_π(Ru → PCy_3) (Figure 5a), whereas a poor correlation (R^2 = 0.47) was found between E_σ(NHC → Ru) and $E_\sigma(PCy_3 \rightarrow Ru)$ (Figure 5b). Taking these observations together, we hypothesize that PCy_3 and

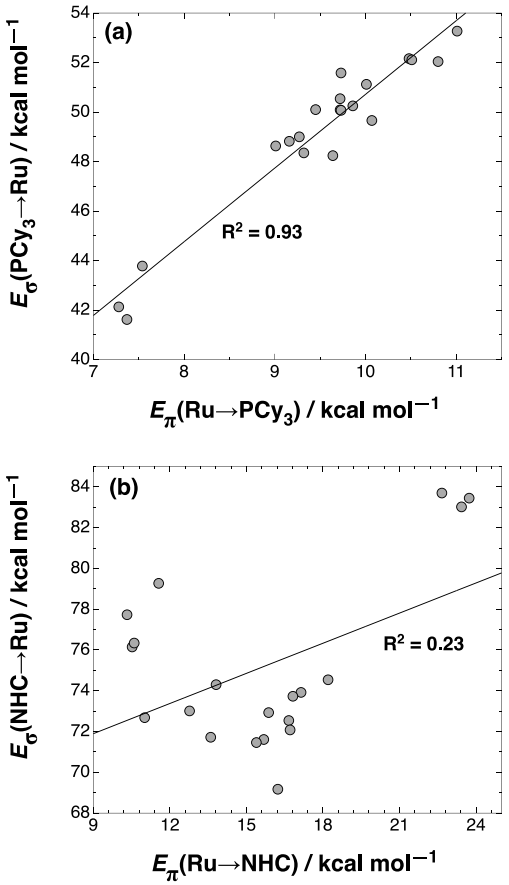

Figure 4. (a) $E_\sigma(PCy_3 \rightarrow Ru)$ vs E_π (Ru → PCy_3) for the Ru−PCy_3 bond and (b) E_σ(NHC → Ru) vs E_π (Ru → NHC) for the Ru−NHC bond in the ruthenium complexes shown in Figure 1.

NHC ligands in the considered ruthenium adducts communicate through π bonding: i.e., the weaker the Ru−PCy_3 π bond, the stronger the Ru−NHC π-bond and *vice versa*. In other words, when there is less π electron density available for PCy_3, the NHC is more π accepting, and thus the Ru−PCy_3 bond is weaker.

For example, among the 20 studied ruthenium adducts, complexes **CAAC1−3** presented the highest E_π for the Ru−NHC bond (22.7−23.7 kcal mol^{-1}) and thus the lowest E_π for the Ru−PCy_3 bond (7.3−7.5 kcal mol^{-1}). On the other hand, **I^{i}Pr^{Me}** presented the lowest E_π for the Ru−NHC bond (10.3 kcal mol^{-1}) and the highest E_π for the Ru−PCy_3 bond (11.0 kcal mol^{-1}). As an end result, in support of our hypothesis, complexes **CAAC1−3** presented weaker Ru−PCy_3 bonds (ΔE_{PCy3} = 7.0−8.2 kcal mol^{-1}), while **I^{i}Pr^{Me}** presented a stronger Ru−PCy_3 bond (ΔE_{PCy3} = 20.2 kcal mol^{-1}). Additionally, as further evidence for our hypothesis, in the studied 20 ruthenium adducts we observed a reasonably good correlation (R^2 = 0.82) between E_π(Ru → PCy_3) and ΔE_{PCy3} and an excellent correlation (R^2 = 0.86) between E_π(Ru → PCy_3) and R(Ru−P) bond lengths, suggesting that the R(Ru−P) distances are indeed indicative of the amount of Ru to PCy_3 back-donation, which in turn determines the lability of the PCy_3 ligand (see Figure S4 in the Supporting Information).

As additional remarks, for the cases of ruthenium adducts **IMes**, **SIMes**, **IPr**, and **SIPr**, it is possible to do a comparison among the different NHCs and their influence on the corresponding Ru−PCy_3 bond strength, ΔE_{PCy3}. At first, it is

https://dx.doi.org/10.1021/acs.organomet.0c00536
Organometallics 2020, 39, 3972−3982

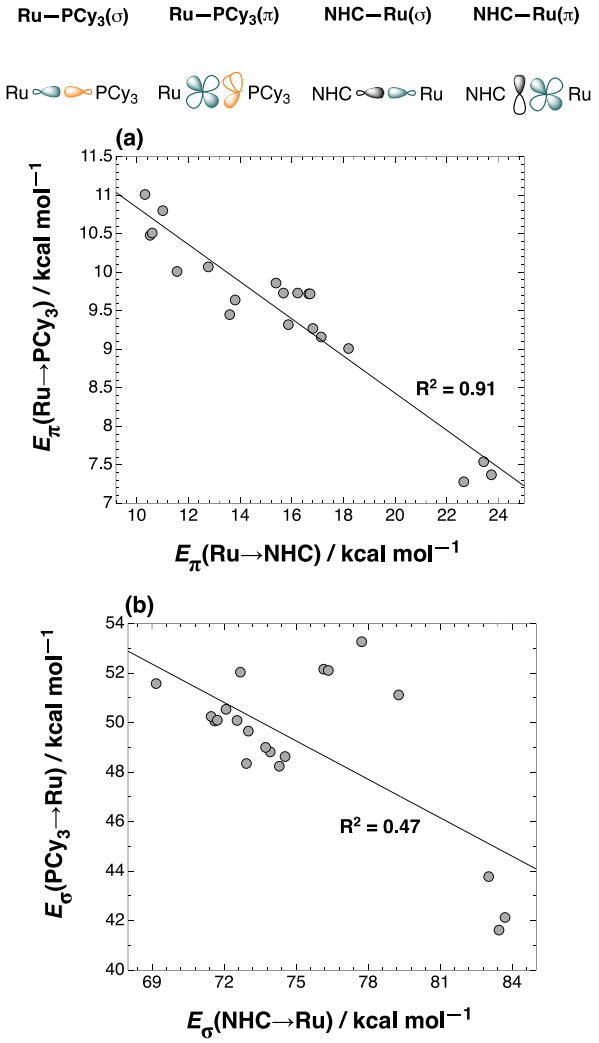

Figure 5. (a) E_π(Ru → NHC) *vs* E_π(Ru → PCy_3) and (b) E_σ(NHC → Ru) *vs* E_σ(PCy_3 → Ru) in the ruthenium complexes shown in Figure 1.

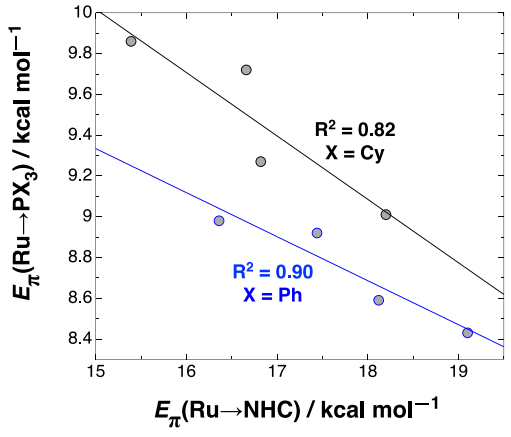

Figure 6. Calculated E_π(Ru→NHC) vs E_π(Ru→PX_3), where X = Cy (black) or Ph (blue), for the ruthenium adducts **IMes**, **SIMes**, **IPr**, and **SIPr**.

evident from Table 1 that the calculated R(Ru−P) distances are slightly shorter in the case of unsaturated NHCs than in the saturated NHCs. This observed trend in bond lengths is in turn reflected in the estimated PCy_3 dissociation energies, ΔE_{PCy3}, as the Ru−PCy_3 bond is stronger (∼2 kcal mol^{-1}) in the case of unsaturated NHCs than in the saturated NHCs.[37] As pointed out in our EDA discussion, the differential strength of the Ru−PCy_3 bonds can be explained from an orbital interaction standpoint. According to EDA, the sum of E_σ and E_π of Ru−PCy_3 bonds (E_{sum}) for unsaturated NHCs (∼60 kcal mol^{-1}) is around 2 kcal mol^{-1} larger than for saturated NHCs (∼58 kcal mol^{-1}).

Next, for ruthenium adducts **IMes**, **SIMes**, **IPr**, and **SIPr**, we substituted PCy_3 by PPh_3 and investigated the corresponding Ru−PPh_3 bond strength, ΔE_{PPh3}, and E_π(Ru→PPh_3). The calculated ΔE_{PPh3} values (21.0−23.0 kcal mol^{-1}) are around 7.0 kcal mol^{-1} higher in energy than the corresponding ΔE_{PCy3} values (13.5−16.0 kcal mol^{-1}). In case of Ru−PCy_3- and Ru−PPh_3-containing adducts, we observed a strong correlation (R^2 = 0.90) between the calculated ruthenium and P bond dissociation energies and R(Ru−P) distances. Additionally, similarly to Ru−PCy_3 adducts, a strong correlation (R^2 = 0.90) was observed between E_π(Ru → NHC) and E_π(Ru → PPh_3) in the four considered Ru−PPh_3 adducts (Figure 6).

Ruthenium═Ylidene Bond. In order to elucidate the bonding and NMR properties of the Ru═ylidene bond for the set of 17 [Ru(═CHR)(NHC)$_x$(PCy_3)$_{2-x}$][Cl]$_2$ first (x = 0)- and second-generation (x = 1) complexes (see Figure 7), our DFT results indicate that the calculated magnetic shielding of the carbene C atom spans a window of 92.8 ppm, complexes **PCy_3-a** (R = CHEt) and **PCy_3-g** (carbazole derivative) being the ones with the lowest and highest calculated ^{13}C magnetic shielding (−139.4 vs − 46.7 ppm, respectively). Further, their experimental chemical shifts have been compared with the calculated shifts, giving an excellent correlation (R^2 = 0.97). This is also added to the fact that the slope and y-intercept variables from the correlation are close to 1 and 0, respectively, which validates the methodology employed by us (including relativistic spin−orbit effects) and provides an almost exact correspondence between the observed and calculated ^{13}C magnetic shieldings. Furthermore, comparison of the DFT vs experimental ^{1}H chemical shifts in this selected set of 17 complexes containing the CHR ylidene motif also exhibits a very good correlation (R^2 = 0.93), with the complex **IMes-e** (R = CHPh) being somewhat out of the trend (see Figure 8 and Figure S7 in the Supporting Information).

As was also observed for the Ru−PCy_3 and Ru−NHC bonds, the main term contributing to the σ(^{13}C) of ylidene C in the Ru═ylidene bond is due to the paramagnetic term, σ_p, spanning a range of 85.7 ppm (diamagnetic and spin−orbit terms exhibit minor contributions).

Since changes in the paramagnetic shielding are due to occupied−occupied but mainly to occupied−virtual molecular orbital (MO) transitions, Figure 9 rationalizes the most important of these for a simple [Ru(═CH_2)(NHC)(PMe_3)]-[Cl]$_2$ model, with NHC = 2,3-dihydro-1*H*-imidazole. As can be seen, optimization under the constraint of C_s symmetry, with the NHC ring lying in the σ_{xy} plane, indicates that for this system σ(^{13}C) = −113.9 ppm and σ_p(^{13}C) = −364.5 ppm. Paramagnetic shielding tensors reveal that the main contributions for σ_p(^{13}C) come from MO transitions projected along the Ox (occupied) and Oy (virtual) axes, with a shielding answer along the Oz axis: $\sigma_{p,zz}$(^{13}C) = −711.8 ppm. This corresponds with the transition between the occupied σ Ru═C bond to the empty $\pi_\parallel$* Ru═C bond, contributing with a total of −69.4 ppm and an energy gap, $\Delta\varepsilon$, of 6.0 eV. In addition, a smaller but also significant contribution comes from

https://dx.doi.org/10.1021/acs.organomet.0c00536
Organometallics 2020, 39, 3972−3982

Table 1. Comparison of Bonding Properties in Ruthenium Adducts IMes, IPr, SIMes, and SIPr

complex	R(Ru−P)/Å	ΔE_{PCy3}/kcal mol^{-1}	E_σ(PCy$_3$→Ru)/kcal mol^{-1}	E_π(Ru→PCy$_3$)/kcal mol^{-1}
IMes	2.503	15.7	50.1	9.7
IPr	2.497	15.6	50.3	9.9
SIMes	2.517	13.4	48.6	9.0
SIPr	2.513	13.4	49.0	9.3

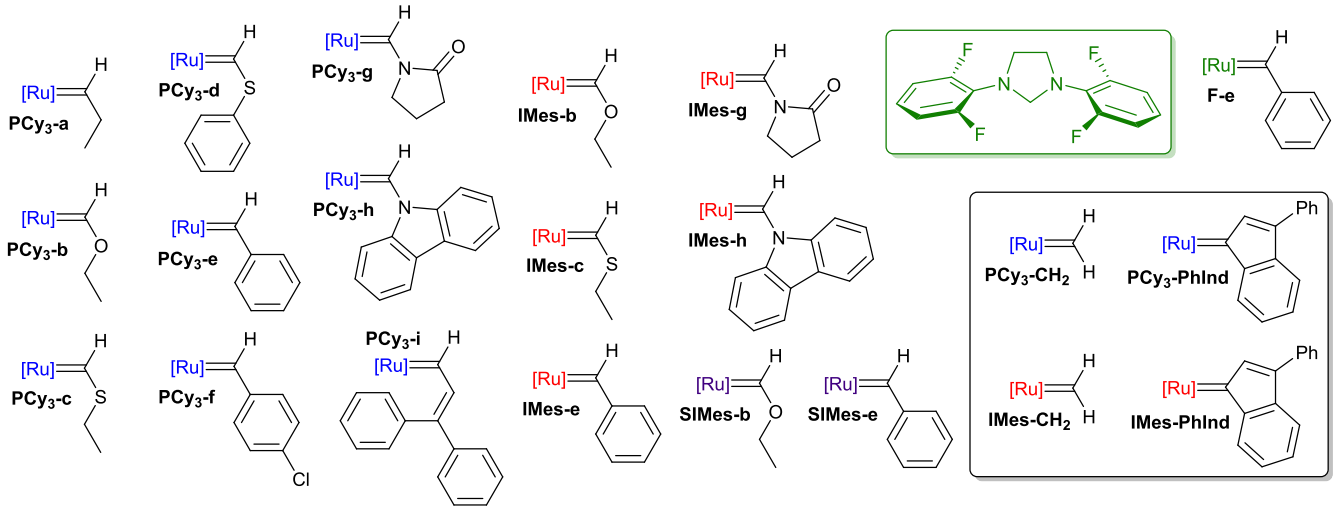

Figure 7. Set of 17 [Ru(=CHR)(NHC)$_x$(PCy$_3$)$_{2-x}$][Cl$_2$] first (x = 0)- and second-generation (x = 1) adducts considered in the second part of this study. [Ru] moieties refer to [Ru(PCy$_3$)$_2$][Cl]$_2$ (blue), [Ru(IMes)(PCy$_3$)][Cl]$_2$ (red), [Ru(SIMes)(PCy$_3$)][Cl]$_2$ (purple), and {Ru[1,3-bis(2,6-difluorophenyl)imidazolidine](PCy$_3$)}[Cl]$_2$ (green). The nomenclature is consistent with these [Ru] moieties. The first- and second-generation (NHC = **IMes**) complexes for methylene and phenyl-indenylidene are also included: **PCy$_3$-CH$_2$**, **PCy$_3$-PhInd**, **IMes-CH$_2$**, and **IMes-PhInd**.

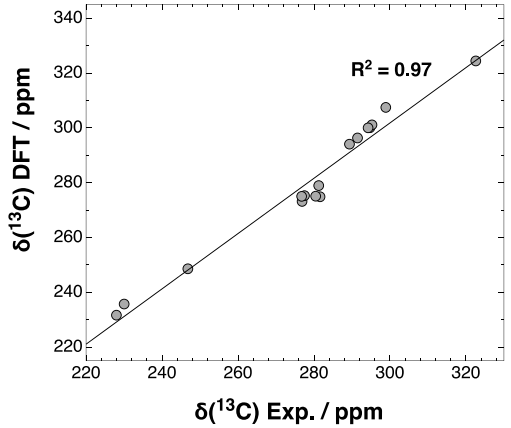

Figure 8. Comparison of experimental vs calculated ^{13}C chemical shifts for the complexes in Figure 7 containing the =CHR motif, using tetramethylsilane (TMS) as reference: $\delta = \sigma_{ref} - \sigma$.

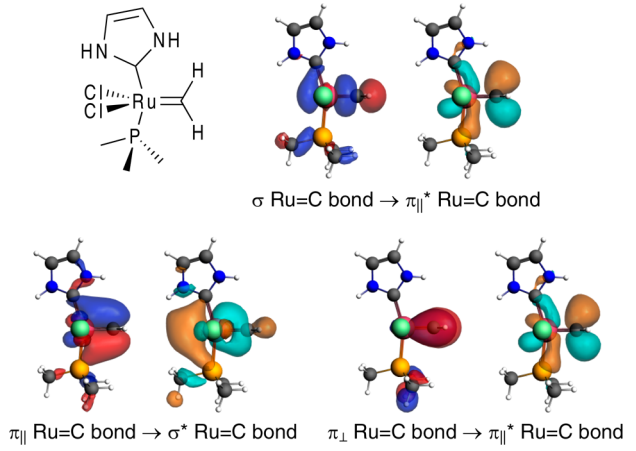

Figure 9. The most significant MO transitions explaining σ_p for the simplest [Ru(=CH$_2$)(NHC)(PMe$_3$)][Cl]$_2$ model, NHC = 2,3-dihydro-1*H*-imidazole.

a transition from the filled $\pi_{\|}$ Ru=C bond to the virtual σ* Ru=C bond, participating with −14.5 ppm and an energy gap of 5.0 eV.

A complete analysis requires the elucidation of the main MOs transitions that respond to the changes occurring in the shielding answer along the Ox axis, since $\sigma_{p,xx}$(^{13}C) = −315.0 ppm. In this case, a $\pi_\perp$ Ru=C bond → $\pi_{\|}$* Ru=C bond transition is showed as the main transition explaining $\sigma_{p,xx}$(^{13}C), contributing with −10.3 ppm and an energy gap of 7.8 eV. Finally, the very low value of $\sigma_{p,yy}$(^{13}C) = −66.6 ppm suggests practically no participation of MOs projected along the Ox and Oz axes.

When we focus on the main σ Ru=C bond → $\pi_{\|}$* Ru=C bond transition for the set of 17 Ru adducts shown at Figure 7 plus the first- and second-generation (NHC = **IMes**) complexes for methylene and phenyl-indenylidene, there is a clear relationship between the energy gap of the MOs involved in such transitions and the calculated ^{13}C magnetic shielding. This reveals the dominant role that they play, exhibiting that the smaller the $\Delta\varepsilon$, the stronger the coupling (deshielded) and *vice versa*. Interestingly, similar adducts that are only differentiated by the presence of two PCy$_3$ ligands (first generation) or one PCy$_3$ and one NHC ligand (second generation) present close values of both $\Delta\varepsilon$ and σ(^{13}C), showing that there is a

https://dx.doi.org/10.1021/acs.organomet.0c00536
Organometallics 2020, 39, 3972−3982

minor influence of such ligands in the NMR response of the ylidene C atom.[38] In addition to this, ^{13}C magnetic shieldings can be grouped on the basis of the nature of the alkylidine group; thus ylidene C atoms directly attached to aromatic C atoms are less shielded than those in which these atoms are bonded to a chalcogen atom such as O or S, and these are less shielded than those directly bonded to a N atom, such as the carbazole and pyrrilidone derivatives. The energy of the empty MOs of the $\pi_{\|}$* Ru=C bond range 1.68 eV over the 21 adducts studied, while the occupied MOs of the σ Ru=C bond range 0.83 eV; thus a larger range of energy is spanned by the virtual MOs. Finally, when both first- and second-generation [Ru]=CH_2 and **PCy_3-a** complexes are excluded, a good correlation (R^2 = 0.78) can be seen, as shown in Figure 10.

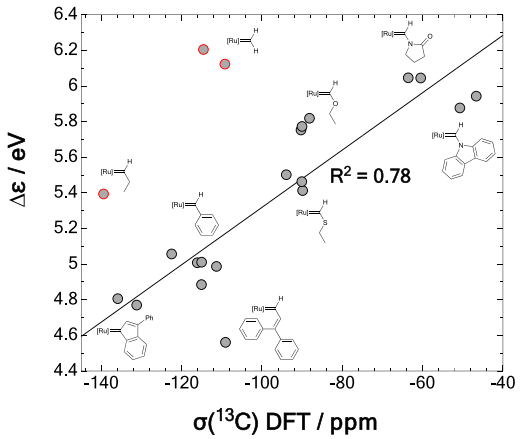

Figure 10. Comparison of energy gap, $\Delta\varepsilon$, vs the calculated ^{13}C magnetic shielding, $\sigma(^{13}C)$, for the MOs involved in the σ Ru=C bond → $\pi_{\|}$* Ru=C bond transition. Points in red are excluded from the regression analysis.

In support of these observations, EDA analyses also shed light on the nature of the Ru=ylidene bond and its relationship with $\sigma(^{13}C)$. For the 21 ruthenium adducts considered, rigidly fragmented into the [Ru(NHC)$_x$(PCy$_3$)$_{2-x}$][Cl]$_2$ (x = 0, 1) and the CHR moieties (including [Ru]=CH_2 and [Ru]=PhInd complexes), it can be seen that the stronger the coupling (low field), the stronger the bond and *vice versa*, [Ru(NHC)$_x$(PCy$_3$)$_{2-x}$][Cl]$_2$ (x = 0, 1) moieties being triplet multiplicity fragments in all cases, while for CHR moieties the singlet vs triplet stability depends on the fragment. This relationship also exhibits a good correlation (R^2 = 0.89, excluding [Ru]=CH_2 and [Ru]=PhInd adducts), with shielding being grouped by alkylidenes and exhibiting a minor influence of the PCy_3 and NHC ligands (see Figure 11).

Previously described by us, calculated Ru−PCy_3 and Ru−NHC bond lengths were found to be good indicators of the corresponding bond strengths. For the case of the Ru=ylidene bond, it is observed that the calculated Ru=C distances also correlate with calculated ^{13}C magnetic shielding, showing two different correlation behaviors: either those adducts in which the carbene C atom is directly attached to another C atom (aromatic or not) presents R^2 = 0.93, with the two [Ru]=PhInd complexes (**PCy_3-PhInd** and **IMes-PhInd**) excluded from this correlation (see Figure 12) or for those cases in which the ylidene C atom is bonded with another heteroatom (O, S, N) or for the two [Ru]=CH_2 complexes (**PCy_3-CH_2**

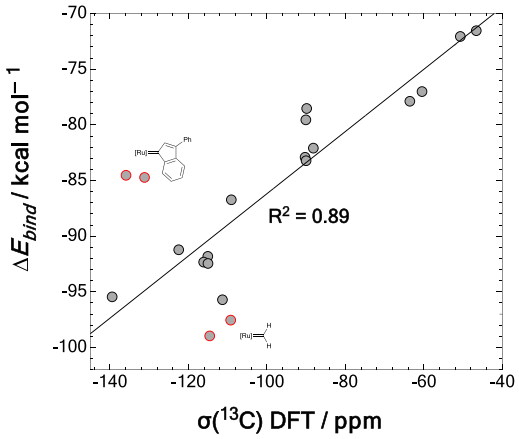

Figure 11. Comparison of the binding energy, ΔE_{bind}, vs the calculated ^{13}C magnetic shielding, $\sigma(^{13}C)$, of the [Ru] and =CHR ylidene fragments. Points in red are excluded from the regression analysis.

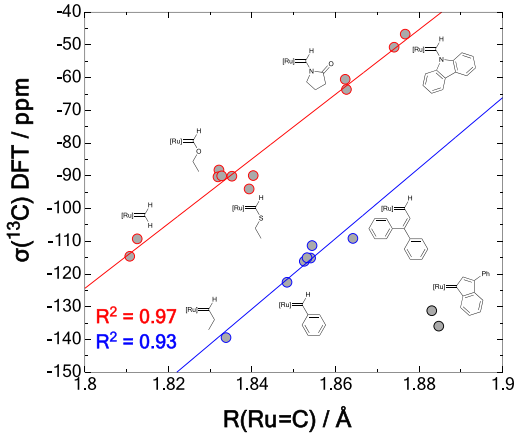

Figure 12. Comparison of the calculated ^{13}C magnetic shielding, $\sigma(^{13}C)$, vs R(Ru=C) bond length. Two correlation behaviors are seen: for those adducts in which carbene C atom is directly attached to another C atom (aromatic or not, blue) and those in which it is bonded with a different heteroatom (red). Points in violet are excluded from the regression analysis.

and **IMes-CH_2**), a very good correlation is also obtained (R^2 = 0.97). On the basis of these two groups, it is seen that a lower field means stronger and shorter Ru=C bonds. However, it is worth mentioning that, for a given Ru=C distance, $\sigma(^{13}C)$ for the Ru=C−C motif is more deshielded than for the case of Ru=C−X (X = O, S, N).

Once the basis of the connectivity between the NMR shielding of the ylidene C atom with the orbital, bonding, and structural properties of the Ru=ylidene bond in the [Ru(=CHR)(NHC)$_x$(PCy$_3$)$_{2-x}$][Cl]$_2$ (x = 0, 1) 16e species is elucidated, an extension of our DFT findings to the initialization process of olefin metathesis establishes some interesting relations.

First of all, Scheme 2 gathers the general mechanism for the formation of the metallacycle compound from the 16e species, passing through PCy_3 dissociation (leading to the so-called 14e species) and through the insertion of one ethylene molecule (coordination intermediate). The metallacycle compound is characterized to have a four-membered ring constituted by the Ru metal, the former ylidene C atom, one C(α), and C′(α) and C′(β) from C_2H_4.

https://dx.doi.org/10.1021/acs.organomet.0c00536
Organometallics 2020, 39, 3972−3982

Scheme 2. General Mechanism for the Formation of the Metallacycle Compound from the 16e Species

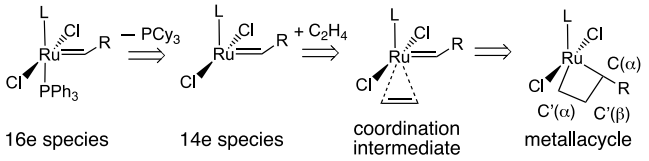

In contrast to what has been recently observed by Gordon et al.[39] in some transition-metal olefin metathesis catalyst complexes, it seems that $\sigma[^{13}C(\alpha)]$ in the metallacycle does not retain some of the alkylidene character (Figure 13a).

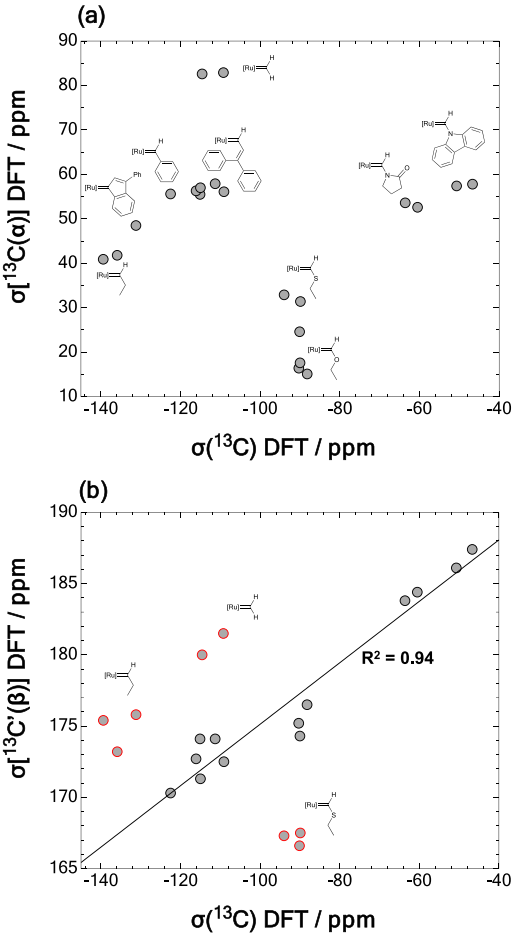

Figure 13. (a) Comparison of calculated ^{13}C magnetic shielding for $C(\alpha)$ in the metallacycle and the carbene C in the 16e species. Groups of points are clustered by colors. (b) Comparison of calculated ^{13}C magnetic shielding for $C'(\beta)$ in the metallacycle and the carbene C in the 16e species. Points in red are excluded from the regression analysis.

Although our work is focused on complexes using the same metal but different bonding environments by modifying the ylidene moiety, we do not observe any trend allowing the correlation of $\sigma[^{13}C(\alpha)]$ before and after cyclization. Indeed, what is observed is that $\sigma[^{13}C(\alpha)]$, ranging in a shielding window of ca. 50 ppm, is distributed by groups, highlighting the importance of the atoms directly bonded to $C(\alpha)$. However, surprising information can be extracted from Figure 13b, in which with the exception of some complexes such as **PCy_3-CH_2**, **IMes-CH_2**, **PCy_3-PhInd**, and **IMes-PhInd** and complexes with sulfur-containing ylidenes a good correlation can be seen ($R^2 = 0.94$) for $\sigma[^{13}C'(\beta)]$ in the metallacycle and $\sigma(^{13}C)$ in the 16e species. However, does this relationship mean that $C'(\beta)$ has the capacity to retain the information from the precatalyst? An additional comparison between $\sigma[^{13}C'(\beta)]$ and $\sigma(^{13}C)$ in the isolated $C'(\beta)H_2{=}C(\alpha)HR$ alkenes demonstrates that this correlation does not come from the entering olefin, which points to validation of our hypothesis.

In this sense, the very low window of $\sigma[^{13}C'(\beta)]$ (ca. 20 ppm) as well as the large number of MO transitions contributing to $\sigma_p[^{13}C'(\beta)]$ does not allow us to establish a clear correlation as we did in Figure 10 between $\Delta\varepsilon$ and $\sigma[^{13}C'(\beta)]$. However, it seems that the nature of this shielding covers σ C−H bond to π^* C−H bond transitions mainly involving $C(\alpha)$ and $C'(\beta)$ atoms with p orbitals from X at $C'(\beta)-C(\alpha)-X$ playing some role in the up- or downfield shielding of $\sigma[^{13}C'(\beta)]$.

CONCLUSIONS

In summary, using DFT calculations we have investigated the electronic nature of Ru−PCy_3 and the Ru−NHC bonds, probing a possible mode of communication between the PCy_3 and NHC ligands for a set of 20 $[Ru(=CH_2)(NHC)(PCy_3)]$-$[Cl]_2$ adducts. Phosphorus NMR shielding derived from calculations correlated well ($R^2 = 0.87$) with the calculated R(Ru−P) bond lengths. The latter was strongly correlated ($R^2 = 0.86$) with the calculated PCy_3 ligand dissociation energies, indicating that the calculated bond lengths are good indicators of the corresponding bond strengths. However, this explanation does not hold for the Ru−NHC bond, as no correlation ($R^2 = 0.09$) was observed between R(Ru−NHC) bond lengths and NHC ligand dissociation energies.

Bond energy decomposition analysis (EDA) indicated a strong correlation ($R^2 = 0.93$) between σ and π orbital interaction energies for the Ru−PCy_3 bond, while a poor correlation ($R^2 = 0.23$) for the Ru−NHC bond was seen. Additionally, we observed an excellent correlation ($R^2 = 0.91$) between π orbital interaction energies of the Ru−PCy_3 and the Ru−NHC bonds, suggesting that both ligands communicate through π-bonding: i.e., a stronger Ru−NHC π bond means a weaker Ru−PCy_3 π bond and *vice versa*. Furthermore, π orbital interaction energies of the PCy_3 ligand were found to be strongly correlated to ΔE_{PCy3} ($R^2 = 0.82$), as well as to the R(Ru−P) bond lengths ($R^2 = 0.95$). These observations indeed reflect the importance of Ru to PCy_3 back-donation, which in turn is regulated by the π-accepting ability of NHCs, in determining the lability of the PCy_3 ligand for the 20 studied ruthenium adducts.

Furthermore, for the set of 17 $[Ru(=CHR)(NHC)_x(PCy_3)_{2-x}][Cl]_2$ first ($x = 0$)- and second-generation ($x = 1$) complexes, our DFT findings hypothesize that changes occurring in the ^{13}C NMR shielding of the Ru=ylidene bond are mainly due to $\sigma(Ru{=}C) \rightarrow \pi^*(Ru{=}C)$ molecular orbital (MO) transitions. In this regard, $\sigma(^{13}C)$ for carbene C of the ylidene moiety correlates with the energy gap of the MOs involved in the aforementioned transition, with the binding energy between the alkylidene and the rest of the Ru fragment, and with the R(Ru=C) bond lengths.

Finally, novel preliminary results shown by us also hypothesize that, during the initial stage of the olefin metathesis reaction, $^{13}C'(\beta)$ NMR shielding from the metallacycle compound retains the NMR information from the

https://dx.doi.org/10.1021/acs.organomet.0c00536
Organometallics 2020, 39, 3972−3982

$\sigma(^{13}C)$ in the 16e species, although it surprisingly does not with the $^{13}C(\alpha)$ NMR shielding, C(α) being the former carbene C form the ylidene moiety.

■ ASSOCIATED CONTENT

Supporting Information

The Supporting Information is available free of charge at https://pubs.acs.org/doi/10.1021/acs.organomet.0c00536.

Extended computational data (PDF)

Cartesian coordinates (XYZ)

■ AUTHOR INFORMATION

Corresponding Authors

Luis Miguel Azofra − *Instituto de Estudios Ambientales y Recursos Naturales (i-UNAT), Universidad de Las Palmas de Gran Canaria (ULPGC), Campus de Tafira, 35017 Las Palmas de Gran Canaria, Spain;* orcid.org/0000-0003-4974-1670; Email: luismiguel.azofra@ulpgc.es

Albert Poater − *Institut de Química Computacional i Catàlisi, Departament de Química, Universitat de Girona, 17003 Girona, Catalonia, Spain;* orcid.org/0000-0002-8997-2599; Email: albert.poater@udg.edu

Luigi Cavallo − *King Abdullah University of Science and Technology (KAUST), KAUST Catalysis Center (KCC), Thuwal 23955-6900, Saudi Arabia;* orcid.org/0000-0002-1398-338X; Email: luigi.cavallo@kaust.edu.sa

Authors

Sai V. C. Vummaleti − *King Abdullah University of Science and Technology (KAUST), KAUST Catalysis Center (KCC), Thuwal 23955-6900, Saudi Arabia*

Ziyun Zhang − *King Abdullah University of Science and Technology (KAUST), KAUST Catalysis Center (KCC), Thuwal 23955-6900, Saudi Arabia*

Complete contact information is available at: https://pubs.acs.org/10.1021/acs.organomet.0c00536

Author Contributions

The manuscript was written through contributions of all authors. All authors have given approval to the final version of the manuscript.

Notes

The authors declare no competing financial interest.

■ ACKNOWLEDGMENTS

A.P. is a Serra Húnter Professor and thanks ICREA Academia 2019 and the Spanish MINECO for project ref PGC2018-097722-B-I00. The authors acknowledge the Universidad de Las Palmas de Gran Canaria (ULPGC) and the King Abdullah University of Science and Technology (KAUST) for support. Gratitude is also due to the KAUST Supercomputing Laboratory using the supercomputer Shaheen II for providing the computational resources.

■ REFERENCES

(1) Arduengo, A. J.; Harlow, R. L.; Kline, M. A Stable Crystalline Carbene. *J. Am. Chem. Soc.* **1991**, *113*, 361−363.

(2) (a) Díez-González, S.; Nolan, S. P. Stereoelectronic Parameters Associated with N-Heterocyclic Carbene (NHC) Ligands: A Quest for Understanding. *Coord. Chem. Rev.* **2007**, *251*, 874−883. (b) Samojłowicz, C.; Bieniek, M.; Grela, K. Ruthenium-Based Olefin Metathesis Catalysts Bearing N-Heterocyclic Carbene Ligands. *Chem. Rev.* **2009**, *109*, 3708−3742. (c) Mercs, L.; Albrecht, M. Beyond Catalysis: N-Heterocyclic Carbene Complexes as Components for Medicinal, Luminescent, and Functional Materials Applications. *Chem. Soc. Rev.* **2010**, *39*, 1903−1912. (d) Janssen-Müller, D.; Schlepphorst, C.; Glorius, F. Privileged Chiral N-Heterocyclic Carbene Ligands for Asymmetric Transition-Metal Catalysis. *Chem. Soc. Rev.* **2017**, *46*, 4845−4854. (e) Peris, E. Smart N-Heterocyclic Carbene Ligands in Catalysis. *Chem. Rev.* **2018**, *118*, 9988−10031.

(3) (a) Jacobsen, H.; Correa, A.; Poater, A.; Costabile, C.; Cavallo, L. Understanding the M(NHC) (NHC = N-Heterocyclic Carbene) Bond. *Coord. Chem. Rev.* **2009**, *253*, 687−703. (b) Jacobsen, H.; Correa, A.; Poater, A.; Costabile, C.; Cavallo, L. Erratum: Understanding the M(NHC) (NHC = N-Heterocyclic Carbene) Bond. *Coord. Chem. Rev.* **2009**, *253*, 2784−2784. (c) Rouen, M.; Queval, P.; Borré, E.; Falivene, L.; Poater, A.; Berthod, M.; Hugues, F.; Cavallo, L.; Baslé, O.; Olivier-Bourbigou, H.; Mauduit, M. Selective Metathesis of α-Olefins from Bio-Sourced Fischer−Tropsch Feeds. *ACS Catal.* **2016**, *6*, 7970−7976. (d) Gimferrer, M.; Salvador, P.; Poater, A. Computational Monitoring of Oxidation States in Olefin Metathesis. *Organometallics* **2019**, *38*, 4585−4592. (e) Poater, A.; Falivene, L.; Urbina-Blanco, C. A.; Manzini, S.; Nolan, S. P.; Cavallo, L. How Does the Addition of Steric Hindrance to a typical N-heterocyclic Carbene Ligand Affect Catalytic Activity in Olefin Metathesis? *Dalton Trans.* **2013**, *42*, 7433−7439. (f) Manzini, S.; Urbina-Blanco, C. A.; Nelson, D. J.; Poater, A.; Lebl, T.; Meiries, S.; Slawin, A. M. Z.; Falivene, L.; Cavallo, L.; Nolan, S. P. Evaluation of an Olefin Metathesis Pre-Catalyst with a Bulky and Electron-Rich N-Heterocyclic Carbene. *J. Organomet. Chem.* **2015**, *780*, 43−48.

(4) (a) Marion, N.; Díez-González, S.; Nolan, S. P. N-Heterocyclic Carbenes as Organocatalysts. *Angew. Chem., Int. Ed.* **2007**, *46*, 2988−3000. (b) Biju, A. T.; Kuhl, N.; Glorius, F. Extending NHC-Catalysis: Coupling Aldehydes with Unconventional Reaction Partners. *Acc. Chem. Res.* **2011**, *44*, 1182−1195.

(5) (a) Hahn, F. E.; Jahnke, M. C. Heterocyclic Carbenes: Synthesis and Coordination Chemistry. *Angew. Chem., Int. Ed.* **2008**, *47*, 3122−3172. (b) Raubenheimer, H. G.; Cronje, S. Carbene Complexes of Gold: Preparation, Medical Application and Bonding. *Chem. Soc. Rev.* **2008**, *37*, 1998−2011. (c) Díez-González, S.; Marion, N.; Nolan, S. P. N-Heterocyclic Carbenes in Late Transition Metal Catalysis. *Chem. Rev.* **2009**, *109*, 3612−3676. (d) Nolan, S. P. The Development and Catalytic Uses of N-Heterocyclic Carbene Gold Complexes. *Acc. Chem. Res.* **2011**, *44*, 91−100. (e) Bellemin-Laponnaz, S.; Dagorne, S. Group 1 and 2 and Early Transition Metal Complexes Bearing N-Heterocyclic Carbene Ligands: Coordination Chemistry, Reactivity, and Applications. *Chem. Rev.* **2014**, *114*, 8747−8774. (f) Hopkinson, M. N.; Richter, C.; Schedler, M.; Glorius, F. An overview of N-heterocyclic carbenes. *Nature* **2014**, *510*, 485. (g) Nesterov, V.; Reiter, D.; Bag, P.; Frisch, P.; Holzner, R.; Porzelt, A.; Inoue, S. NHCs in Main Group Chemistry. *Chem. Rev.* **2018**, *118*, 9678−9842. (h) Krehl, S.; Geißler, D.; Hauke, S.; Kunz, O.; Staude, L.; Schmidt, B. The Catalytic Performance of Ru-NHC Alkylidene Complexes: PCy_3 Versus Pyridine as the Dissociating Ligand. *Beilstein J. Org. Chem.* **2010**, *6*, 1188−1198.

(6) Grubbs, R. H. Olefin-Metathesis Catalysts for the Preparation of Molecules and Materials (Nobel Lecture). *Angew. Chem., Int. Ed.* **2006**, *45*, 3760−3765.

(7) Chauvin, Y. Olefin Metathesis: The Early Days (Nobel Lecture). *Angew. Chem., Int. Ed.* **2006**, *45*, 3740−3747.

(8) Schrock, R. R. Multiple Metal-Carbon Bonds for Catalytic Metathesis Reactions (Nobel Lecture). *Angew. Chem., Int. Ed.* **2006**, *45*, 3748−3759.

(9) Wu, Z.; Nguyen, S. T.; Grubbs, R. H.; Ziller, J. W. Reactions of Ruthenium Carbenes of the Type $(PPh_3)_2(X)_2Ru{:}CH{-}CH{:}CPh_2$ (X = Cl and CF_3COO) with Strained Acyclic Olefins and Functionalized Olefins. *J. Am. Chem. Soc.* **1995**, *117*, 5503−5511.

(10) (a) Huang, J.; Stevens, E. D.; Nolan, S. P.; Petersen, J. L. Olefin Metathesis-Active Ruthenium Complexes Bearing a Nucleophilic Carbene Ligand. *J. Am. Chem. Soc.* **1999**, *121*, 2674−2678. (b) Scholl, M.; Ding, S.; Lee, C. W.; Grubbs, R. H. Synthesis and Activity of a

New Generation of Ruthenium-Based Olefin Metathesis Catalysts Coordinated with 1,3-Dimesityl-4,5-dihydroimidazol-2-ylidene Ligands. *Org. Lett.* **1999**, *1*, 953−956. (c) Weskamp, T.; Kohl, F. J.; Hieringer, W.; Gleich, D.; Herrmann, W. A. Highly Active Ruthenium Catalysts for Olefin Metathesis: The Synergy of N-Heterocyclic Carbenes and Coordinatively Labile Ligands. *Angew. Chem., Int. Ed.* **1999**, *38*, 2416−2419. (d) Poater, A.; Cavallo, L. A Comprehensive Study of Olefin Metathesis Catalyzed by Ru-based Catalysts. *Beilstein J. Org. Chem.* **2015**, *11*, 1767−1780. (e) Poater, A.; Ragone, F.; Correa, A.; Cavallo, L. Comparison of Different Ruthenium-Alkylidene Bonds in the Sctivation Step with N-Heterocyclic Carbene Ru-Catalysts for Olefins Metathesis. *Dalton Trans.* **2011**, *40*, 11066−11069. (f) Bielawski, C. W.; Grubbs, R. H. Highly Efficient Ring-Opening Metathesis Polymerization (ROMP) Using New Ruthenium Catalysts Containing N-Heterocyclic Carbene Ligands. *Angew. Chem., Int. Ed.* **2000**, *39*, 2903−2906.

(11) Nelson, D. J.; Nolan, S. P. Quantifying and understanding the electronic properties of N-heterocyclic carbenes. *Chem. Soc. Rev.* **2013**, *42*, 6723−6753.

(12) Tolman, C. A. Steric Effects of Phosphorus Ligands in Organometallic Chemistry and Homogeneous Catalysis. *Chem. Rev.* **1977**, *77*, 313−348.

(13) (a) Poater, A.; Cosenza, B.; Correa, A.; Giudice, S.; Ragone, F.; Scarano, V.; Cavallo, L. SambVca: A Web Application for the Calculation of the Buried Volume of N-Heterocyclic Carbene Ligands. *Eur. J. Inorg. Chem.* **2009**, *2009*, 1759−1766. (b) Clavier, H.; Nolan, S. P. Percent Buried Volume for Phosphine and N-Heterocyclic Carbene Ligands: Steric Properties in Organometallic Chemistry. *Chem. Commun.* **2010**, *46*, 841−861.

(14) Setiawan, D.; Kalescky, R.; Kraka, E.; Cremer, D. Direct Measure of Metal-Ligand Bonding Replacing the Tolman Electronic Parameter. *Inorg. Chem.* **2016**, *55*, 2332−2344.

(15) (a) Falivene, L.; Credendino, R.; Poater, A.; Petta, A.; Serra, L.; Oliva, R.; Scarano, V.; Cavallo, L. SambVca 2. A Web Tool for Analyzing Catalytic Pockets with Topographic Steric Maps. *Organometallics* **2016**, *35*, 2286−2293. (b) Falivene, L.; Cao, Z.; Petta, A.; Serra, L.; Poater, A.; Oliva, R.; Scarano, V.; Cavallo, L. Towards the Online Computer-Aided Design of Catalytic Pockets. *Nat. Chem.* **2019**, *11*, 872−879.

(16) (a) Huynh, H. V. Electronic Properties of N-Heterocyclic Carbenes and Their Experimental Determination. *Chem. Rev.* **2018**, *118*, 9457−9492. (b) Veenboer, R. M. P.; Azofra, L. M.; Gasperini, D.; Collado, A.; Cordes, D. B.; Slawin, A. M. Z.; Cavallo, L.; Nolan, S. P. Regression Analysis of Properties of [Au(IPr)(CHR_2)] Complexes. *Dalton Trans.* **2019**, *48*, 7693−7703.

(17) (a) Tulloch, A. A. D.; Danopoulos, A. A.; Kleinhenz, S.; Light, M. E.; Hursthouse, M. B.; Eastham, G. Structural Diversity in Pyridine-N-Functionalized Carbene Copper(I) Complexes. *Organometallics* **2001**, *20*, 2027−2031. (b) Jacobsen, H.; Correa, A.; Costabile, C.; Cavallo, L. π-Acidity and π-Basicity of N-Heterocyclic Carbene Ligands. A Computational Assessment. *J. Organomet. Chem.* **2006**, *691*, 4350−4358. (c) Andrada, D. M.; Holzmann, N.; Hamadi, T.; Frenking, G. Direct Estimate of the Internal π-Donation to the Carbene Centre Within N-heterocyclic Carbenes and Related Molecules. *Beilstein J. Org. Chem.* **2015**, *11*, 2727−2736.

(18) Dorta, R.; Stevens, E. D.; Scott, N. M.; Costabile, C.; Cavallo, L.; Hoff, C. D.; Nolan, S. P. Steric and Electronic Properties of N-Heterocyclic Carbenes (NHC): A Detailed Study on Their Interaction with $Ni(CO)_4$. *J. Am. Chem. Soc.* **2005**, *127*, 2485−2495.

(19) (a) Nitsch, J.; Wolters, L. P.; Fonseca Guerra, C.; Bickelhaupt, F. M.; Steffen, A. Enhanced π-Back-Donation as a Way to Higher Coordination Numbers in d^{10} [$M(NHC)_n$] Complexes: A DFT Study. *Chem. - Eur. J.* **2017**, *23*, 614−622. (b) Khramov, D. M.; Lynch, V. M.; Bielawski, C. W. N-Heterocyclic Carbene-Transition Metal Complexes: Spectroscopic and Crystallographic Analyses of π-Back-Bonding Interactions. *Organometallics* **2007**, *26*, 6042−6049. (c) Sanderson, M. D.; Kamplain, J. W.; Bielawski, C. W. Quinone-annulated N-Heterocyclic Carbene-Transition-Metal Complexes: Observation of π-Backbonding Using FT-IR Spectroscopy and Cyclic Voltammetry. *J. Am. Chem. Soc.* **2006**, *128*, 16514−16515.

(20) Vummaleti, S. V. C.; Nelson, D. J.; Poater, A.; Gómez-Suárez, A.; Cordes, D. B.; Slawin, A. M. Z.; Nolan, S. P.; Cavallo, L. What Can NMR Spectroscopy of Selenoureas and Phosphinidenes Teach Us About the π-Accepting Abilities of N-Heterocyclic Carbenes? *Chem. Sci.* **2015**, *6*, 1895−1904.

(21) Fantasia, S.; Petersen, J. L.; Jacobsen, H.; Cavallo, L.; Nolan, S. P. Electronic Properties of N-Heterocyclic Carbene (NHC) Ligands: Synthetic, Structural, and Spectroscopic Studies of (NHC)Platinum-(II) Complexes. *Organometallics* **2007**, *26*, 5880−5889.

(22) Back, O.; Henry-Ellinger, M.; Martin, C. D.; Martin, D.; Bertrand, G. ^{31}P NMR Chemical Shifts of Carbene-Phosphinidene Adducts as an Indicator of the π-Accepting Properties of Carbenes. *Angew. Chem., Int. Ed.* **2013**, *52*, 2939−2943.

(23) Liske, A.; Verlinden, K.; Buhl, H.; Schaper, K.; Ganter, C. Determining the π-Acceptor Properties of N-Heterocyclic Carbenes by Measuring the ^{77}Se NMR Chemical Shifts of Their Selenium Adducts. *Organometallics* **2013**, *32*, 5269−5272.

(24) Dutta, S.; Maity, B.; Thirumalai, D.; Koley, D. Computational Investigation of Carbene-Phosphinidenes: Correlation between ^{31}P Chemical Shifts and Bonding Features to Estimate the π-Back-donation of Carbenes. *Inorg. Chem.* **2018**, *57*, 3993−4008.

(25) (a) Nelson, D. J.; Collado, A.; Manzini, S.; Meiries, S.; Slawin, A. M. Z.; Cordes, D. B.; Nolan, S. P. Methoxy-Functionalized N-Heterocyclic Carbenes. *Organometallics* **2014**, *33*, 2048−2058. (b) Nelson, D. J.; Nahra, F.; Patrick, S. R.; Cordes, D. B.; Slawin, A. M. Z.; Nolan, S. P. Exploring the Coordination of Cyclic Selenoureas to Gold(I). *Organometallics* **2014**, *33*, 3640−3645.

(26) (a) Marchione, D.; Belpassi, L.; Bistoni, G.; Macchioni, A.; Tarantelli, F.; Zuccaccia, D. The Chemical Bond in Gold(I) Complexes with N-Heterocyclic Carbenes. *Organometallics* **2014**, *33*, 4200−4208. (b) Gaggioli, C. A.; Bistoni, G.; Ciancaleoni, G.; Tarantelli, F.; Belpassi, L.; Belanzoni, P. Modulating the Bonding Properties of N-Heterocyclic Carbenes (NHCs): A Systematic Charge-Displacement Analysis. *Chem. - Eur. J.* **2017**, *23*, 7558−7569. (c) Gregori, L.; Sorbelli, D.; Belpassi, L.; Tarantelli, F.; Belanzoni, P. Alkyne Activation with Gold(III) Complexes: A Quantitative Assessment of the Ligand Effect by Charge-Displacement Analysis. *Inorg. Chem.* **2019**, *58*, 3115−3129.

(27) Ciancaleoni, G.; Scafuri, N.; Bistoni, G.; Macchioni, A.; Tarantelli, F.; Zuccaccia, D.; Belpassi, L. When the Tolman Electronic Parameter Fails: A Comparative DFT and Charge Displacement Study of $[(L)Ni(CO)_3]^{0/-}$ and $[(L)Au(CO)]^{0/+}$. *Inorg. Chem.* **2014**, *53*, 9907−9916.

(28) Azofra, L. M.; Veenboer, R. M. P.; Falivene, L.; Vummaleti, S. V. C.; Poater, A.; Nolan, S. P.; Cavallo, L. Quantifying Electronic Similarities Between NHC-Gold(I) Complexes and Their Isolobal Imidazolium Precursors. *Phys. Chem. Chem. Phys.* **2019**, *21*, 15615−15622.

(29) (a) Becke, A. D. Density-functional Exchange-Energy Approximation with Correct Asymptotic Behavior. *Phys. Rev. A: At., Mol., Opt. Phys.* **1988**, *38*, 3098−3100. (b) Perdew, J. P. Density-Functional Approximation for the Correlation Energy of the Inhomogeneous Electron Gas. *Phys. Rev. B: Condens. Matter Mater. Phys.* **1986**, *33*, 8822−8824.

(30) Van Lenthe, E.; Baerends, E. J. Optimized Slater-Type Basis Sets for the Elements 1−118. *J. Comput. Chem.* **2003**, *24*, 1142−1156.

(31) (a) Becke, A. D. A multicenter numerical integration scheme for polyatomic molecules. *J. Chem. Phys.* **1988**, *88*, 2547−2553. (b) Franchini, M.; Philipsen, P. H. T.; Visscher, L. The Becke Fuzzy Cells Integration Scheme in the Amsterdam Density Functional Program Suite. *J. Comput. Chem.* **2013**, *34*, 1819−1827.

(32) (a) Lenthe, E. v.; Baerends, E. J.; Snijders, J. G. Relativistic Regular Two-Component Hamiltonians. *J. Chem. Phys.* **1993**, *99*, 4597−4610. (b) van Lenthe, E.; Baerends, E. J.; Snijders, J. G. Relativistic Total Energy Using Regular Approximations. *J. Chem. Phys.* **1994**, *101*, 9783−9792. (c) van Lenthe, E.; Ehlers, A.; Baerends,

https://dx.doi.org/10.1021/acs.organomet.0c00536
Organometallics 2020, 39, 3972−3982

E.-J. Geometry Optimizations in the Zero Order Regular Approximation for Relativistic Effects. *J. Chem. Phys.* **1999**, *110*, 8943−8953.
(33) (a) Schreckenbach, G.; Ziegler, T. Calculation of NMR Shielding Tensors Using Gauge-Including Atomic Orbitals and Modern Density Functional Theory. *J. Phys. Chem.* **1995**, *99*, 606−611. (b) Schreckenbach, G.; Ziegler, T. The Calculation of NMR Shielding Tensors Based on Density Functional Theory and the Frozen-Core Approximation. *Int. J. Quantum Chem.* **1996**, *60*, 753−766. (c) Schreckenbach, G.; Ziegler, T. Calculation of NMR Shielding Tensors Based on Density Functional Theory and a Scalar Relativistic Pauli-type Hamiltonian. The Application to Transition Metal Complexes. *Int. J. Quantum Chem.* **1997**, *61*, 899−918.
(34) Mitoraj, M. P.; Michalak, A.; Ziegler, T. A Combined Charge and Energy Decomposition Scheme for Bond Analysis. *J. Chem. Theory Comput.* **2009**, *5*, 962−975.
(35) Gaggioli, C. A.; Belpassi, L.; Tarantelli, F.; Harvey, J. N.; Belanzoni, P. Spin-Forbidden Reactions: Adiabatic Transition States Using Spin-Orbit Coupled Density Functional Theory. *Chem. - Eur. J.* **2018**, *24*, 5006−5015.
(36) (a) Minenkov, Y.; Occhipinti, G.; Jensen, V. R. Metal-Phosphine Bond Strengths of the Transition Metals: A Challenge for DFT. *J. Phys. Chem. A* **2009**, *113*, 11833−11844. (b) Lummiss, J. A. M.; Higman, C. S.; Fyson, D. L.; McDonald, R.; Fogg, D. E. The Divergent Effects of Strong NHC Donation in Catalysis. *Chem. Sci.* **2015**, *6*, 6739−6746.
(37) Minenkov, Y.; Occhipinti, G.; Heyndrickx, W.; Jensen, V. R. The Nature of the Barrier to Phosphane Dissociation from Grubbs Olefin Metathesis Catalysts. *Eur. J. Inorg. Chem.* **2012**, *2012*, 1507−1516.
(38) Falivene, L.; Cavallo, L. Theoretical NMR Spectroscopy of N-Heterocyclic Carbenes and Their Metal Complexes. *Coord. Chem. Rev.* **2017**, *344*, 101−114.
(39) (a) Gordon, C. P.; Culver, D. B.; Conley, M. P.; Eisenstein, O.; Andersen, R. A.; Copéret, C. π-Bond Character in Metal-Alkyl Compounds for C-H Activation: How, When, and Why? *J. Am. Chem. Soc.* **2019**, *141*, 648−656. (b) Gordon, C. P.; Yamamoto, K.; Liao, W.-C.; Allouche, F.; Andersen, R. A.; Copéret, C.; Raynaud, C.; Eisenstein, O. Metathesis Activity Encoded in the Metallacyclobutane Carbon-13 NMR Chemical Shift Tensors. *ACS Cent. Sci.* **2017**, *3*, 759−768.

https://dx.doi.org/10.1021/acs.organomet.0c00536
Organometallics 2020, 39, 3972−3982